SCIENCE CHINA Materials ARTICLES

mater.scichina.com link.springer.com

Published online 7 August 2017 | https://doi.org/10.1007/s40843-017-9071-y
Sci China Mater 2018, 61(4): 607–618

SPECIAL ISSUE: Advances in Metallic Biomaterials

In vitro degradation and biocompatibility of Mg-Li-Ca alloys—the influence of Li content

Lanyue Cui[1,2†], Lu Sun[1,2†], Rongchang Zeng[1,2*], Yufeng Zheng[3*] and Shuoqi Li[1,2]

ABSTRACT **Mg-Li based alloys hold much attention as potential biomedical materials due to their excellent ductility. A reduced mechanical strength and concern for biocompatibility are exhibited for Mg-Li binary alloys due to the presence of Li element. Addition of the Ca element into Mg-Li alloys leads to an improvement in mechanical strength and biocompatibility. In the present work, the microstructure, mechanical property and corrosion behaviors of three kinds (α, α+β, β) of as-extruded Mg-Li (1, 9 and 15 wt.%)-1Ca alloys were investigated using optical microscope, X-ray diffraction (XRD), tensile, immersion and electrochemical polarization measurements. *In vitro* biocompatibility was evaluated by cytotoxicity assays, hemolysis and four coagluation tests. The results indicated that the Mg-1Li-1Ca and Mg-15Li-1Ca alloys were characterized by α-Mg and β-Li phases besides Mg_2Ca particles, respectively; while the Mg-9Li-1Ca by dual (α-Mg+β-Li) phase together with Mg_2Ca phase. The Mg-1Li-1Ca alloy had the highest ultimate tensile strength (UTS) and yield strength (YS) and the lowest elongation (EL) to failure (10.1±1.24%) as well. The EL for the Mg-9Li-1Ca alloy was the highest (52.2±0.01%). The long-term immersion tests revealed a decrease in corrosion resistance with increasing Li content. The results of cytotoxicity assays clearly showed that the Mg-Li-Ca alloys demonstrated no toxicity to L-929 cells in 10% concentration of extracts. The Mg-1Li-1Ca alloy also exhibited an acceptable hemolysis ratio. The results of four coagulation tests designated no sign of thrombogenicity for the Mg-Li-Ca alloys except for the Mg-15Li-1Ca alloy.**

Keywords: magnesium alloy, degradation, mechanical property, biocompatibility, biomaterial

INTRODUCTION

Mg alloys are considered as appropriate candidates for biodegradable cardiovascular stents and bone replacement metallic implants due to their excellent biocompatibility and osteoconductivity [1–6]. While the existing commercial Mg alloys cannot meet the needs for mechanical properties, corrosion resistance and biocompatibility of the degradable implants [7–9].

Currently, Mg-Li alloys have attracted much attention as their super *in vivo* corrosion resistance [3,10–12]. The commercial Mg-Li alloys, such as LAE442, have been applied in the field of aerospace by virtue of their exceptionally low density (1.35–1.65 g cm^{-3}), high specific strength and good formability [3,13]. Addition of Li can stabilize the body-centered cubic (BCC) (β phase) at the expense of the hexagonal closed-packed (HCP) solid solution of Mg (α phase). Mg-Li alloys can be classified into three types (α, α+β, β) by the Li content and crystal structure [14,15]. When the Li content is less than 5.7 wt.%, the Mg-Li alloy is composed of α phase, a HCP Mg crystal structure, in which the Li atoms are solid-soluted. The alloy with a content of Li higher than 10.3 wt.% is composed of the β phase, a BCC Li crystal structure, in which the Mg is solid-soluted [16]. The β phase is well known to exhibit a good formability but possesses a relatively low strength and working-harden capacity. An Mg-Li alloy with composing of 5.7–10.3 wt.% Li is supposed to give a dual phase microstructure of both HCP (α) and BCC (β) structures with super plasticity [10].

The investigation on biomedical Mg-Li alloys can trace back to the report from Witte [3,17], who [3] once implanted four kinds of Mg alloys (AZ31, AZ91, LAE442

[1] College of Materials Science and Engineering, Shandong University of Science and Technology, Qingdao 266590, China
[2] State Key Laboratory of Mining Disaster Prevention and Control Co-founded by Shandong Province and the Ministry of Science and Technology, Shandong University of Science and Technology, Qingdao 266590, China
[3] Department of Materials Science and Engineering, College of Engineering, Peking University, Beijing 100871, China
[†] These authors contributed equally to this work.
[*] Corresponding authors (emails: rczeng@foxmail.com (Zeng R); yfzheng@pku.edu.cn (Zheng Y))

and WE43) into femora of guinea pigs for 6 and 18 weeks. Surprisingly, the LAE442 designates the most excellent *in vivo* corrosion resistance among these alloys. Subcutaneous bubbles have been found surrounding all the degrading Mg implants. The results of skin sensitizing potential show that the LAE442 alloy exhibits anaphylactic reactions similar to the Ti6Al4V alloy [18]. The *in vivo* results of the LAE442 alloy and MgF_2-coated LAE442 [19] show that no adverse host reactions and infections have been clinically observed during the postoperative follow up. All results of the blood examination for cereal third transaminase, aspartate transaminase, alkaline phosphatase, creatinine, total protein as well as four cell counts (erythrocytes, leucocytes, hematocrit, hemoglobin) are in the physiological range for the rabbits. The histopathology analyses of synovial tissue, kidneys and liver tissue disclose that just a few cases exhibit mild toxicity, including one case that formed a fibrotic tissue with local areas of cartilage metaplasia; two cases that had a granular cell infiltration; one case that had suffered from focal chronic lympho-plasmocytic interstitial nephritis and nine cases that reveal minimal focal infiltrations of heterophil granulocytes of unknown origin [19]. Therefore, the reason for these results remains unclear.

In addition, few studies have been made for *in vitro* and *in vivo* corrosion, corrosion protection and biocompatibility of LAE442 and Mg-Li-(Al)-(RE) alloys [14,19,20]. Zhou *et al.* [14] revealed that the addition of rare earth elements results in a decrease in corrosion resistance of Mg-Li-based alloys due to the presence of the $CeAl_2$ intermetallic compound. After a five-day incubation, vascular smooth muscle cell proliferation was suppressed on the Mg-3.5Li-2/4Al-2RE and Mg-8.5Li-2Al-2RE alloys, while tolerated on the Mg-3.5Li, Mg-8.5Li and Mg-8.5Li-1Al alloys in the absence of RE. The Mg-Li-based alloys showed no significantly reduced cell viabilities and acceptable hemolysis ratios except for the Mg-8.5Li-2Al-2RE alloy. In addition, the *in vitro* and *in vivo* investigations manifested the good biocompatibility and eligible toxicity for the forged Mg-13Li-X (Mg-Li-Al-Zn-Ca-Sr) alloys [21].

The aforementioned results reveal that the Mg-Li-Al-RE alloys, such as the LAE442 alloy, are not the optimum candidate due to the higher contents of Al and rare earth elements, which are toxic to body tissue. Our previous studies [6,10,11,22] and others [23] indicate that Mg-Li-Ca alloys may be one of the candidate materials. Ca is one of the major elements in bones, the second large amount of cations in human body, and has the potential to further reduce the density of Mg-Li alloys, refine the microstructure and improve the mechanical strength by forming the intermetallic compound Mg_2Ca [24]. Ca also reduces the oxidation of Mg during melting and improves their high temperature strength, but leads to the brittleness of alloys when Ca content is over 2 wt.% [24]. Generally, it is well suggested [25] that the Mg-Ca alloys with Ca addition between 0.8 and 1.0 wt.% show a good biocompatibility, low corrosion rate and suitable elastic modulus and mechanical strength as well. Our previous study [10] shows that the naturally formed oxide film on the dual phase Mg-9Li-1Ca alloy is composed of four layers: the outer layer is composed of Li_2O, LiOH and Li_2CO_3; the second layer contains LiOH, Li_2O_2, Li_2CO_3, $MgCO_3$ and LiH; the third layer consists of oxides (Li_2O_2, Li_2O, MgO and CaO); and the bottom layer includes the oxides at grain boundaries and in the α-Mg, β-Li phases. In addition, Mg-1.33Li-0.6Ca alloys have both corrosion resistance and mechanical properties superior to Mg-0.54Ca alloys [10], indicating that the introduction of Li element into Mg-Ca alloys is beneficial for the enhancement in corrosion resistance of Mg-Ca alloys. Introduction of Ca element leads to an improvement in yield strength of Mg-Li alloy. Furthermore, our previous investigation [26] discloses that the Mg-1Li-1Ca alloy is non-cytotoxic to osteoblasts, and the cytotoxicity of the Mg-1Li-1Ca alloy is lower than that of pure Mg and AZ31B alloy. The Mg-1Li-1Ca alloy has no impact on osteoblast proliferation and shows good biocompatibility [6]. Unfortunately, little information is available in the literature with regard to the corrosion, mechanical property and biocompatibility of the ternary Mg-Li-Ca alloys [27]. Furthermore, Kashyap *et al.* [23] showed that Mg-4Li-1Ca (LC41) alloy exhibits substantially high specificed strength of 142 kN m kg^{-1} owing to its low density and combined effect of grain boundary strengthening and dispersion strengthening in the presence of Mg_2Ca phase. LC41 alloy also shows an increase in the overall bio-corrosion resistance in simulated body fluid as a result of a change in the corrosion mechanism from localized to uniform corrosion [23].

In view of the virtues of Ca and Li elements, three kinds of Mg-Li-Ca alloys with different contents of Li were fabricated, including Mg-1Li-1Ca, Mg-9Li-1Ca and Mg-15Li-1Ca, all of the content are in weight percentage (wt. %). The purpose of this paper is to investigate the microstructure, mechanical property, and corrosion resistance as well as biocompatibility of the three types of the Mg-Li-Ca alloys to take further insight into the influence of Li on *in vitro* corrosion, tensile property and biocompatibility. Thus, the novel Mg-Li-Ca alloys may be

promising for application in bone implants.

EXPERIMENTAL SECTION

Materials preparation

The chemical compositions of the as-extruded Mg-Li-Ca are listed in Table 1. The as-extruded Mg-Li-Ca alloys specimens were cut into square pieces (20 mm×20 mm×2 mm) for microstructure characterization, corrosion measurements, and the specimens were further cutting to the size of 10 mm×10 mm×2 mm for cytotoxicity and hemocompatibility tests. Before the tests, all specimens were ground to 2000 grit and cleaned in ethanol and distilled water, then dried by warm air. For the cytotoxicity tests, the samples were sterilized by ultraviolet radiation for at least 2 h.

Microstructure characterization

All the specimens were mechanically polished and cleaned in ethanol, dried by warm air. After the specimens were etched with a 4% HNO_3/ethanol solution, the metallographic structure of specimens was observed by virtue of optical microscopy. X-ray diffractometer (XRD, Rigaku D/MAX2500PC) using Cu Kα radiation (λ = 0.154 nm) was adopted to identify the phases present in the as-extruded Mg-Li-Ca alloys. The scanning angle ranged from 10° to 90° at a scan rate of 6° min^{-1}. The densities of the alloys were obtained by:

$$\rho = \frac{M}{V}, \quad (1)$$

where M and V were the mass and volume of the alloys, respectively.

Tensile test

The samples with a gauge length of 25 mm and a width of 6 mm were machined. The tensile tests were performed on a CMT5105 type tensile machine at a strain rate of 3 mm min^{-1} at room temperature according to the standard GB/T228-2002. An average of at least three samples was taken for each group.

Electrochemical measurements

Before the electrochemical tests, all samples were ground with SiC sand papers up to 2000 grit and cleaned in ethanol and distilled water, then dried by warm air. Electrochemical experiments were carried out with a traditional three-electrode cell using a potentiostat (PAR Model 2273, Princeton Applied Research). The specimens acted as the working electrode; while a saturated calomel electrode (SCE) and a platinum plate were the reference and auxiliary electrodes, respectively. All the polarization measurements were performed in a water-bath at a temperature of 37.0±0.5°C in Hank's balanced salt solution (HBSS: 8.0 g L^{-1} NaCl, 0.4 g L^{-1} KCl, 0.14 g L^{-1} $CaCl_2$, 0.1 g L^{-1} $MgCl_2{\cdot}6H_2O$, 0.35 g L^{-1} $NaHCO_3$, 1.0 g L^{-1} $C_6H_6O_6$ (glucose), 0.06 g L^{-1} $MgSO_4{\cdot}7H_2O$, 0.06 g L^{-1} KH_2PO_4, 0.06 g L^{-1} $Na_2HPO_4{\cdot}12H_2O$) at a scan rate of 1 mV s^{-1} [9]. The area of the working electrode exposed to the solution was 1 cm^2. A triple measurement was performed for each group.

Table 1 Chemical compositions of the as-extruded Mg-Li-Ca alloys (wt.%)

Alloys	Li	Ca	Mg
Mg-1Li-1Ca	1.26	0.95	Balance
Mg-9Li-1Ca	9.29	0.88	Balance
Mg-15Li-1Ca	15.0	1.34	Balance

Immersion tests

The hydrogen evolution tests were conducted by placing the sample under an inverted funnel, which was connected to a graduated burette [28,29]. The detailed process was recorded in our previous study [6,11,28,29]. The samples were immersed in HBSS at 37.0±0.5°C for three weeks.

Contact angle measurement

Water contact angle (CA) of the Mg-Li-Ca samples was measured by CA analyzer (Kino SL200B). For each sample, the measurements were carried out in triplicate.

Cytotoxicity tests

The cytotoxicity tests were performed through an indirect contact assay. Murine fibroblast cells (L-929) were cultured in the Dulbecco's modified Eagle's medium (DMEM) with 10% fetal bovine serum, 100 μg mL^{-1} penicillin and 100 μg mL^{-1} sterptomycin at 37°C in a humidified atmosphere of 5% CO_2. Extracts were prepared using a serum-free DMEM with a surface area to extraction medium ratio of 1 cm^2 mL^{-1} in a humidified atmosphere with 5% CO_2 at 37°C for 72 h. The supernatant fluid was withdrawn, centrifuged to prepare the extracts; parts of these extracts were drawn out and diluted by fresh serum-free DMEM into 10% volume ratio extracts. Then the extracts were refrigerated at 4°C before the cytotoxicity testing. Cells were incubated in 96-well flat-bottomed cell culture plates at 5×10^3 cells in 100 μL of medium per well and incubated for 24 h. The medium was then replaced with 100 μL of extracts, i.e., 100 μL of

negative control (medium alone) or 100 μL of a positive control (medium containing 10% dimethysulfoxide). After incubating the cells in a humidified atmosphere with 5% CO_2 at 37°C for 1, 3 and 5 days, 10 μL of cell counting kit (cck8) solution was added to each well and kept for 4 h. Then the spectrophotometrical absorbance of each well was measured with a microplate reader (Bio-RAD 680) at 545 nm.

Hemolysis tests

Healthy human blood (anticoagulant was 3.8 wt.% sodium citric acid) was extracted from volunteers. Normal saline was used to dilute the blood at a ratio of 4:5 by volume. The Mg-Li-Ca alloys were dipped into the separate standard tubes containing 10 mL of normal saline, which had previously been incubated in a water bath at 37°C for 30 min. Then 0.2 mL of the diluted blood was added to the standard tubes and the mixtures were incubated at 37°C for 60 min. Similarly, normal saline solution was used as a negative control and deionized water served as a positive control. Afterward, the samples were removed and all the tubes were centrifuged at 3000 rpm for 5 min. The supernatant from each tube was transferred to a well in a 96-well plate, where the absorbance was measured with a microplate reader (Bio-RAD680) at 545 nm. The hemolysis percentage was calculated based on an average of three replicates:

$$\text{Hemolysis} = \text{OD(test)-OD(negative control)}/\text{OD(positive control)-OD(negative control)} \times 100\%. \quad (2)$$

Four coagulation tests

Four coagulation tests include the tests for prothrombin time (PT), activated partial thromboplatin time (APTT), thrombin time (TT) and fibinogen (FIB). Healthy human blood (anticoagulant was 3.8 wt.% sodium citric acid) was extracted from volunteers. The Mg-Li-Ca alloys were dipped into the separate standard tubes containing 2 mL of blood for 1 h. Then, the samples were removed out from the tubes, and the remained blood was centrifuged for 15 min at 3000 rpm. The supernatant from each tube was tested by the automated coagulation analyzer.

Surface characterization

The cell adhesion on the samples and surface morphologies after the immersion were characterized using an electron probe microanalyzer (EPMA, JXA-8230).

RESULTS

Microstructure evolution

The microstructure was characterized by re-crystallized α-Mg grains and intermetallic Mg_2Ca phases for the extruded Mg-1Li-1Ca alloy (Fig. 1a); duplex phases, including the α and β phases, together with Mg_2Ca phase (Fig. 1b) for the Mg-9Li-1Ca alloy [10]; the β and Mg_2Ca phases for the Mg-15Li-1Ca alloy (Fig. 1c). The intermetallic compounds Mg_2Ca are dispersed in both the grain interiors and grain boundaries. For the Mg-9Li-1Ca alloy, the dispersed Mg_2Ca particles are embedded at the interface between the α-Mg phase and β-Li phase in the extruded alloy along the extrusion direction [10]. No Li_2Ca exists in the alloys [10]. The constituents in microstructure of the samples are further demonstrated by the XRD patterns, as shown in Fig. 2.

Mechanical properties

The tensile stress-stain curves with the corresponding ultimate tensile strength (UTS), yield strength (YS) and elongation (EL) to failure for Mg-Li-Ca alloys are shown in Fig. 3. Both YS and UTS of the Mg-1Li-1Ca alloy are the highest among the Mg-Li-Ca alloys, but the EL is the lowest. The YS and UTS of Mg-9Li-1Ca and Mg-15Li-1Ca alloys are very close, while the ELs of both alloys are enhanced significantly. Particularly, the dual phase Mg-9Li-1Ca alloy has the highest EL of 53%.

Electrochemical polarization

The potentiodynamic polarization curves are shown in

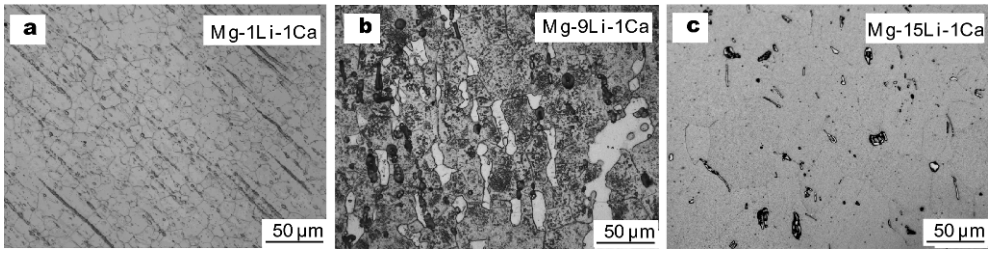

Figure 1 Optical micrographs of the (a) Mg-1Li-1Ca, (b) Mg-9Li-1Ca and (c) Mg-15Li-1Ca alloys.

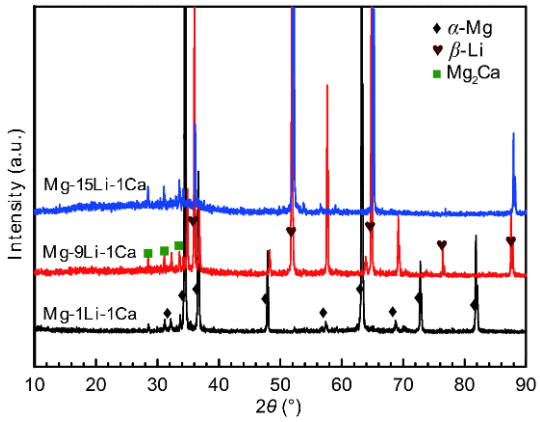

Figure 2 XRD patterns of the Mg-Li-Ca alloys.

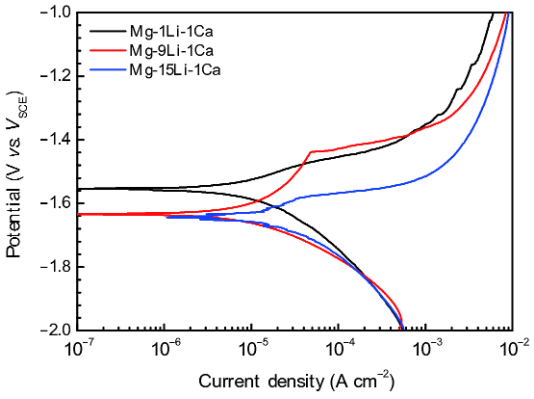

Figure 4 Polarization curves of the Mg-Li-Ca alloys in HBSS.

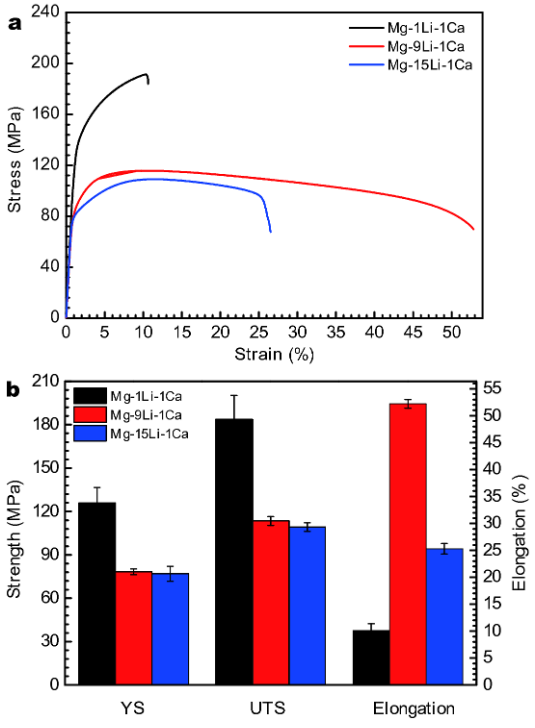

Figure 3 The (a) tensile stress-stain curves and (b) corresponding UTS, YS and EL values for Mg-Li-Ca alloys.

Fig. 4. The corresponding electrochemical parameters are given in Table 2. It was observed that the corrosion current density (i_{corr}) increased with the increase of the Li content, indicating the corrosion resistance was decreased for the Mg-Li-Ca alloys. The Mg-1Li-1Ca alloy and Mg-9Li-1Ca alloy have a lower i_{corr} compared with the Mg-15Li-1Ca alloy, ascribed to the formation of the carbonates (i.e., Li_2CO_3, $MgCO_3$ and $CaCO_3$) in air and deposition of the self-inhibited corrosion product film consisted of LiOH, $Mg(OH)_2$, $CaCO_3$, $MgCO_3$ and $Ca_xMg_y(PO_4)_z$ in HBSS [10]. The Mg-15Li-1Ca alloy shows the fastest corrosion rate, which might be related to the peeling off of the thick corrosion product layer [30].

Cytotoxicity

Fig. 5 shows the cell viability of L-929 cells expressed as a percentage of the viability of cells cultured in the negative control after an incubation for 1, 3 and 5 days in the extracts of the samples. Wang *et al.* [31] recommended a dilution range for the extracts to perform cytotoxicity evaluation between 6 and 10. ISO recommended cell lines (L929) showed no significant difference in cytotoxicity evaluation compared to the primary cells, indicating that the use of these cell lines in priority was acceptable. Under 10% concentration of the extracted solutions, thus, it can be seen that: (1) no obvious differences existed in the L929 cell viability between different culture periods, with all cell viability being higher than 75% after the 5 day incubation. (2) All of the extracts promoted cell proliferation on day 1, whereas the cell viabilities were significantly reduced on day 3 and 5. This was attributed to the inhibiting effect of degradation products such as $Mg(OH)_2$, LiOH, as well as the Li^+ ions. (3) The Mg-15Li-1Ca alloy revealed a lower viability than the Mg-1Li-1Ca and Mg-9Li-1Ca on day 1, which can be ascribed to the rapid oxidation and more release of Li^+ ions.

Hemocompatibility

Fig. 6 shows the hemolysis percentage of the investigated samples. Only the hemolysis ratio of the Mg-1Li-1Ca alloy is lower than 5%, a judging criterion for excellent blood compatibility [16]; whereas the other materials

Table 2 Electrochemical parameters of Mg-Li-Ca alloys

Materials	Density (g cm^{-3})	E_{corr} (V *vs.* SCE)	i_{corr} (μA cm^{-2})	P_w (mm year^{-1})
Mg-1Li-1Ca	1.68±0.21	−1.55	6.49	1.48
Mg-9Li-1Ca	1.63±0.27	−1.63	7.04	2.92
Mg-15Li-1Ca	1.51±0.11	−1.64	14.71	6.26

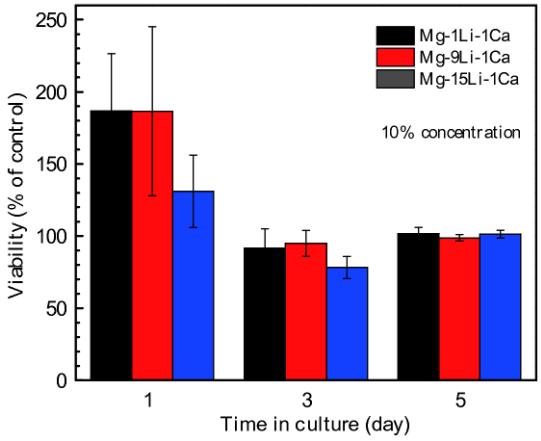

Figure 5 L-929 cell viability after cultured in 10% concentrations of the extracts and positive control for 1, 3 and 5 days.

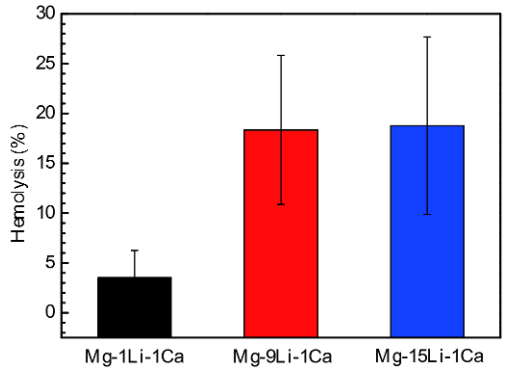

Figure 6 Hemolysis rates of Mg-Li-Ca alloys.

exhibit considerably high hemolysis in contact with whole blood for 60 min. The results might be attributed to the high pH value and high concentration of Mg^{2+} and Li^{+} ions released from the dissolution of the Mg-9Li-1Ca and Mg-15Li-1Ca alloys. Generally, pH ≥ 10 is reported to lead to the serious hemolysis [32]. Li [33] indicated that a 10^{-3} mol L^{-1} concentration of Mg^{2+} ions cannot result in the hemolysis. For the Mg-9Li-1Ca and Mg-15Li-1Ca alloys, the fast degradation rate leads to the Mg^{2+} concentration higher than 10^{-3} mol L^{-1} (pH > 9.975 [34]), then the erythrocytes dissolve and hemoglobin is freed, which may be one of the reasons for the high hemolysis ratio.

The results of four coagulation tests, including PT (Fig. 7a), APT (Fig. 7b), TT (Fig. 7c) and FIB (Fig. 7d), reveal that the Mg-1Li-1Ca and Mg-9Li-1Ca alloys can prolong the coagulation time effectively. These results can be attributed to the antagonism of Mg^{2+} and Ca^{2+} ions. Since thrombin activation requires Ca^{2+} ions, it is quite possible that Mg^{2+} ions compete with Ca^{2+} ions for the binding sites at the thrombin molecules. Thus, the degenerated thrombin cannot activate the clotting factor [35,36].

DISCUSSION

Influence of Li content on mechanical properties

With the development of the biomedical materials, scientists are devoted to developing new Mg-based alloys with low/no toxicity levels and good mechanical properties for biological applications. Taking this consideration in mind, Mg-Li alloys have been developed and investigated. The typical YS and EL of various published investigations on mechanical properties of Mg-Li alloys concerning biomaterials applications are summarized in Fig. 8. This collection covers both the influence of material composition and the die-casting conditions. As summarized, most of the Mg-Li alloys have a YS of less than 150 MPa and EL of wide range (0.4–53%). Among these Mg-Li alloys, Mg-14Li alloys normally exhibit the highest YS and the best EL. Mg-9Li alloys are promising because not only are they the second strongest ductile alloy system, but their corrosion rates can also be greatly reduced by utilizing certain strategies, as described in a later section [10,15,16,23,27,37–41]. In comparison, the novel Mg-1Li-1Ca has the similar YS and EL with the Mg-1Li-1Ca-1Y alloy. Both of them have a similar YS and EL. The Mg-9Li-1Ca has a comparable higher EL with most of the Mg-9Li binary alloy, which is promising for bone implants.

Influence of Li content on cell adhesion and biocompatibility

The adhered platelets on Mg-1Li-1Ca alloy keep a nearly round shape with some pseudopodia-like structures. Their pseudopodia-like structures adhere to the surface of

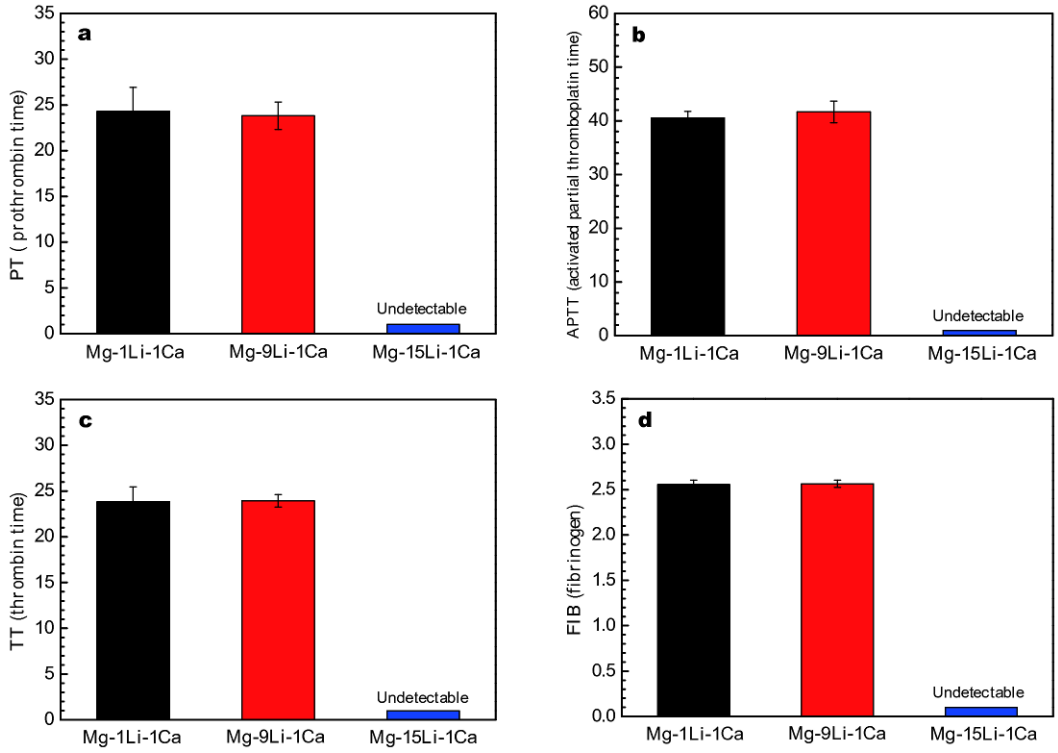

Figure 7 Results of four coagulation tests of Mg-Li-Ca alloys: (a) PT, (b) APTT, (c) TT and (d) FIB.

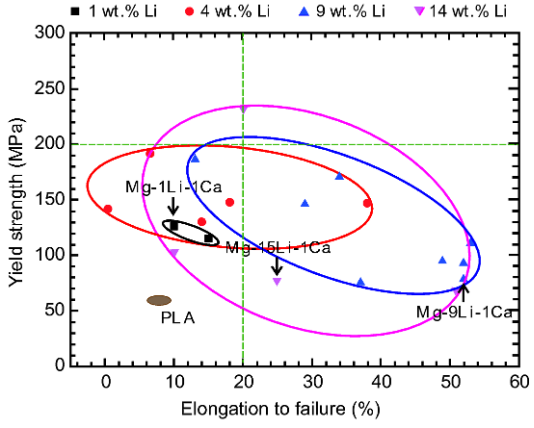

Figure 8 Typical YS and EL of representative biodegradable Mg-Li alloys.

the Mg-1Li-1Ca substrate yet (Fig. 9a). In addition, more and more platelets adhere to the surface of the Mg-9Li-1Ca and Mg-15Li-1Ca samples, whereas almost all platelets distorted seriously with the increase of the Li content, implying positive activation and thrombogenicity (Fig. 9b, c). The hydrogen generated from the corrosion process may accelerate the platelets adhesion because the increased bubble nucleons affect the haemoglobin in blood and contact with the platelets [42].

The surface wettability is very important for hemocompatibility of biomedical materials. The sequence of the CAs of three metals from high to low is: Mg-9Li-1Ca (54.16±3.55°) > Mg-1Li-1Ca (47.60±5.57°)>Mg-15Li-1Ca (17.07±2.55°) (Fig. 10), revealing that the Mg-15Li-1Ca has the best hydrophilicity, while Mg-9Li-1Ca is the worst among the three metals.

Many researches show that [35,43–45] high hydrophilicity contributes to cell adhesion on the surface. The weak and reversible adsorption of hydrophilic effect makes for adapting the structure of the materials to cell growth. The hydrophilic effect also impedes the adhering of platelets so that it is effective to prevent the platelet thrombosis [31,39]. Nevertheless, for the hydrophobic surface, the conformation of protein changes more seriously due to the selective adsorption of *r*-globulin and fibrinogen [40,41]. Thus, the anticoagulation property does not depend on the intensity of the hydrophilicity. It is the microstructure that affects the property of the anticoagulation and cell adhesion.

Influence of Li content on corrosion behaviour

The hydrogen evolution rates (HERs) of the samples for a 419-h immersion are illustrated in Fig. 11. It can be seen

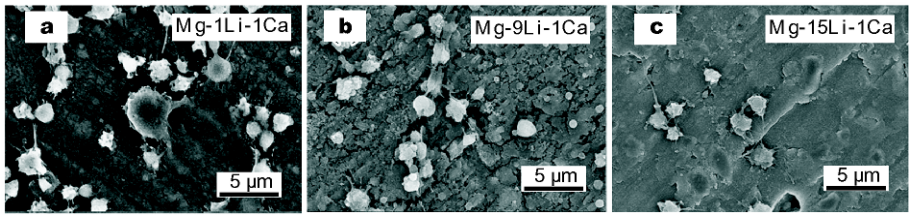

Figure 9 Morphology of platelets adhering to the (a) Mg-1Li-1Ca, (b) Mg-9Li-1Ca and (c) Mg-15Li-1Ca.

Figure 10 The CAs of the (a) Mg-1Li-1Ca, (b) Mg-9Li-1Ca and (c) Mg-15Li-1Ca.

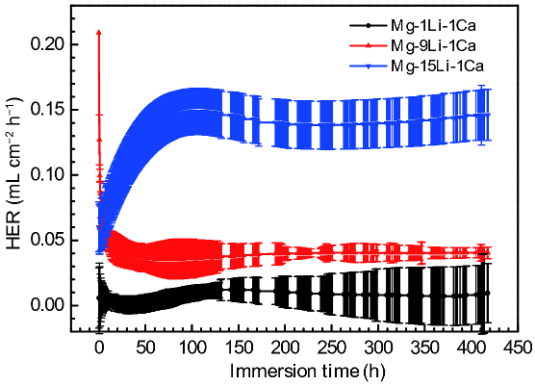

Figure 11 HERs of the Mg-Li-Ca alloys as a function of immersion time in HBSS.

that the HER of the Mg-1Li-1Ca alloy remains at lowest level throughout the whole immersion time. The Mg-9Li-1Ca alloy exhibits a faster HER than the Mg-1Li-1Ca alloy, but much slower than the Mg-15Li-1Ca alloy. Therefore, it is suggested that the HERs decreases with a decrease in Li content of the Mg-Li-Ca alloys. This finding is in pronounced agreement with the result of the electrochemical polarization (Fig. 4). But the variation in HERs between the Mg-9Li-1Ca alloy and Mg-1Li-1Ca alloy is much smaller than that between the Mg-15Li-1Ca alloy and Mg-9Li-1Ca alloy. The result is ascribed to the oxide film and corrosion product film on the Mg-Li-Ca alloys.

In comparison with the as-extruded Mg-1.35Ca alloy (0.064 mL cm^{-2} h^{-1}) [24], the obtained Mg-1Li-1Ca and Mg-9Li-1Ca alloy present a HER of 0.004 and 0.052 mL cm^{-2} h^{-1} after an 8-h immersion, respectively. The HER of as-extruded Mg-1Ca is about 1.4 mL cm^{-2} h^{-1} [46], which is also higher than the mentioned Mg-Li-Ca alloys. Thus, the addition of appropriate amount of Li element is beneficial to the corrosion resistance of the Mg alloys.

Fig. 12 shows the corrosion morphologies of the sample surfaces after immersion in HBSS for 14 days. For the Mg-1Li-1Ca alloy, it can be seen that integrity of the corrosion product films on the samples is maintained and river-bed-like cracks emerge on the sample surface as a result of shrinkage of the corrosion products during drying (Fig. 12a). The Mg-9Li-1Ca alloy is subjected to a mild attack (Fig. 12b). In particular, the Mg-15Li-1Ca alloys suffered from more serious corrosion, a layer of thick and loose corrosion products could be found on the surface (Fig. 12c). Combining with the cross-sectional images of the corrosion product layer (Fig. 13), it can be seen that the corrosion product layer of the Mg-1Li-1Ca has the largest thickness (Fig. 13a). Interestingly, the Mg-9Li-1Ca alloy possesses the thinnest and densest corrosion product layer (Fig. 13b).

The XRD patterns of the corrosion products reveal the

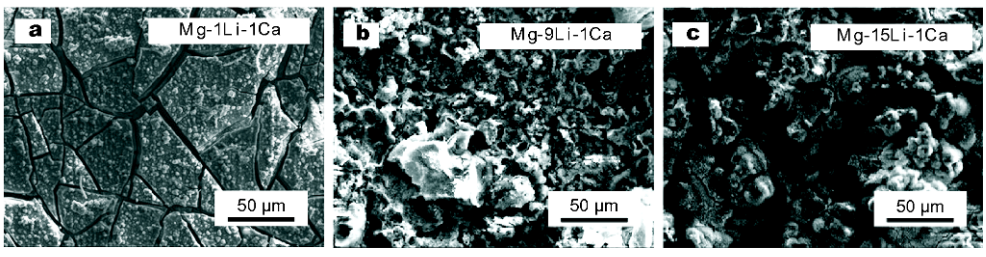

Figure 12 SEM micrographs of the (a) Mg-1Li-1Ca, (b) Mg-9Li-1Ca and (c) Mg-15Li-1Ca after immersion in HBSS for 419 h.

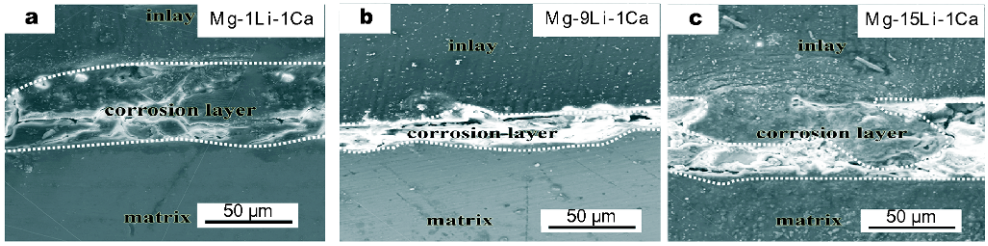

Figure 13 Cross-sectional SEM images of the (a) Mg-1Li-1Ca, (b) Mg-9Li-1Ca and (c) Mg-15Li-1Ca after an immersion of 14 days.

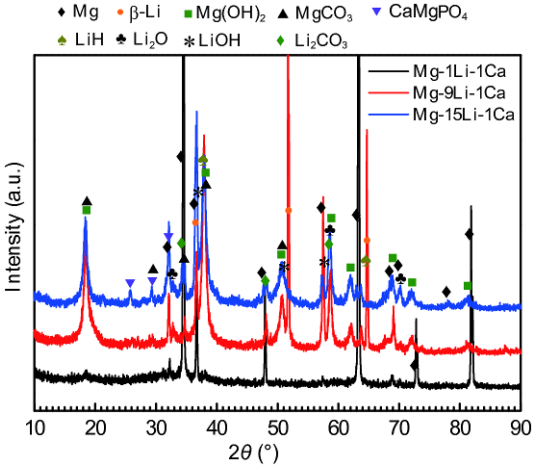

Figure 14 XRD patterns of corrosion products on the surface of the (a) Mg-1Li-1Ca, (b) Mg-9Li-1Ca and (c) Mg-15Li-1Ca after immersion in HBSS for 14 days.

dominant corrosion product $Mg(OH)_2$ formed on all the samples (Fig. 14), except that the $CaMgPO_4$ deposited from the HBSS on the surface of Mg-9Li-1Ca and Mg-15Li-1Ca alloys. In combination with the SEM micrographs (Fig. 12) and cross-sectional SEM images (Fig. 13), a new dense $Mg(OH)_2$ and $CaMgPO_4$ coating deposited on the surface of all Mg-Li-Ca alloys. Note that, the $CaMgPO_4$ coating of the Mg-1Li-1Ca cannot be detected due to its lowest content. The $CaMgPO_4$ coating has a better protection for the substrates, which leads to a smaller variation in HER between the Mg-1Li-1Ca and the Mg-9Li-1Ca [47,48]. But for the Mg-15Li-1Ca alloy, Li exhibits greater mobility and activity in the oxide film, and easily reacts with O_2 to form Li_2O in the loose outer layer of the sample, and therefore, the high Li content accelerates the corrosion of the Mg alloys. The major reactions are as followings:

$$Mg \rightarrow Mg^{2+} + 2e^-, \quad (3)$$

$$2H_2O + 2e^- \rightarrow 2OH^- + H_2\uparrow, \quad (4)$$

$$Mg^{2+} + 2OH^- \rightarrow Mg(OH)_2\downarrow, \quad (5)$$

$$HCO_3^- + OH^- \rightarrow CO_3^{2-} + H_2O, \quad (6)$$

$$Mg^{2+} + CO_3^{2-} \rightarrow MgCO_3\downarrow, \quad (7)$$

$$H_2PO_4^- + OH^- \rightarrow HPO_4^{2-} + H_2O, \quad (8)$$

$$HPO_4^{2-} + OH^- \rightarrow PO_4^{3-} + H_2O, \quad (9)$$

$$xCa^{2+} + yMg^{2+} + zPO_4^{3-} \rightarrow Ca_xMg_y(PO_4)_z, \quad (10)$$

$$4Li + O_2 \rightarrow 2Li_2O, \quad (11)$$

$$2Li + H_2O \rightarrow Li_2O + H_2\uparrow, \quad (12)$$

$$Li_2O + H_2O \rightarrow 2LiOH, \quad (13)$$

$$Li_2O + CO_2 \rightarrow Li_2CO_3. \quad (14)$$

CONCLUSIONS

Three kinds of Mg-Li-Ca alloys including Mg-1Li-1Ca, Mg-9Li-1Ca and Mg-15Li-1Ca alloys were investigated for future biodegradable application in virtue of their excellent ductility.

(1) The Mg-1Li-1Ca alloy consists of the α-Mg and Mg_2Ca phases. The Mg-9Li-1Ca is composed of α-Mg, β-Li and Mg_2Ca phases, while the Mg-15Li-1Ca alloy contains β-Li and Mg_2Ca phases.

(2) The Mg-1Li-1Ca alloy has the highest UTS and YS and the lowest EL as well. The Mg-9Li-1Ca alloy with a duplex structure possesses the highest EL. The Mg-15Li-1Ca alloy has a UTS and YS, which is slightly inferior to the Mg-9Li-1Ca alloy, and an EL of 25.3%. Namely, addition of Li leads to a reduction in mechanical strength and an enhancement in ductility of the Mg-Li-Ca alloys, which with a dual phase is up to 52.2%.

(3) The increase addition of Li gives rise to a decreased corrosion resistance of Mg-Li-Ca alloys in Hank's solution. The long-term immersion demonstrated that the Mg-9Li-1Ca alloy possessed lower HER due to the formation of a thin layer of $Mg(OH)_2$, $CaMgPO_4$, $MgCO_3$ deposits. While the high HER of Mg-15Li-1Ca may be ascribed to the delamination of the loose corrosion product layer, which cannot provide an effective protection.

(4) The Mg-1Li-1Ca alloy had no toxic risks for medical

devices to the L-929 cells in 10% concentration of extracts. Similarly, only the Mg-1Li-1Ca alloy exhibited acceptable hemolysis ratio. No sign of thrombogenicity was found in all experimental Mg-Li-Ca alloys.

Received 7 May 2017; accepted 3 July 2017; published online 7 August 2017

1 Wang J, Smith CE, Sankar J, *et al.* Absorbable magnesium-based stent: physiological factors to consider for *in vitro* degradation assessments. Regen Biomater, 2015, 2: 59–69
2 Gu XN, Li SS, Li XM, *et al.* Magnesium based degradable biomaterials: a review. Front Mater Sci, 2014, 8: 200–218
3 Witte F, Kaese V, Haferkamp H, *et al. In vivo* corrosion of four magnesium alloys and the associated bone response. Biomaterials, 2005, 26: 3557–3563
4 Wang W, Wan P, Liu C, *et al.* Degradation and biological properties of Ca-P contained micro-arc oxidation self-sealing coating on pure magnesium for bone fixation. Regen Biomater, 2015, 2: 107–118
5 Zheng YF, Gu XN, Witte F. Biodegradable metals. Mater Sci Eng-R-Rep, 2014, 77: 1–34
6 Zeng RC, Cui L, Jiang K, *et al. In vitro* corrosion and cytocompatibility of a microarc oxidation coating and poly(l-lactic acid) composite coating on Mg-1Li-1Ca alloy for orthopedic implants. ACS Appl Mater Interfaces, 2016, 8: 10014–10028
7 Zeng R, Dietzel W, Zettler R, *et al.* Microstructural evolution and delayed hydride cracking of FSW-AZ31 magnesium alloy during SSRT. Trans Nonferrous Met Soc China, 2014, 24: 3060–3069
8 Wang HX, Guan SK, Wang X, *et al. In vitro* degradation and mechanical integrity of Mg-Zn-Ca alloy coated with Ca-deficient hydroxyapatite by the pulse electrodeposition process. Acta Biomater, 2010, 6: 1743–1748
9 Gu X, Zheng Y, Zhong S, *et al.* Corrosion of, and cellular responses to Mg-Zn-Ca bulk metallic glasses. Biomaterials, 2010, 31: 1093–1103
10 Zeng RC, Sun L, Zheng YF, *et al.* Corrosion and characterisation of dual phase Mg-Li-Ca alloy in Hank's solution: the influence of microstructural features. Corrosion Sci, 2014, 79: 69–82
11 Zeng RC, Guo XL, Liu C L, *et al.* Study on corrosion of medical Mg-Ca and Mg-Li-Ca alloys. Acta Metall Sin Engl Lett, 2011, 47, 1477–1482
12 Zeng R, Sun X, Song Y, *et al.* Influence of solution temperature on corrosion resistance of Zn-Ca phosphate conversion coating on biomedical Mg-Li-Ca alloys. Trans Nonferrous Met Soc China, 2013, 23: 3293–3299
13 Jiang B, Liu X, Wu R, *et al.* Microstructures and mechanical properties of various Mg-Li wrought alloys. J Shanghai Jiaotong Univ (Sci), 2012, 17: 297–300
14 Zhou WR, Zheng YF, Leeflang MA, *et al.* Mechanical property, biocorrosion and *in vitro* biocompatibility evaluations of Mg-Li-(Al)-(RE) alloys for future cardiovascular stent application. Acta Biomater, 2013, 9: 8488–8498
15 Leeflang MA, Dzwonczyk JS, Zhou J, *et al.* Long-term biodegradation and associated hydrogen evolution of duplex-structured Mg-Li-Al-(RE) alloys and their mechanical properties. Mater Sci Eng-B, 2011, 176: 1741–1745
16 Leeflang M, Zhou J, Duszczyk J. Deformability and extrusion behavior of magnesium-lithium binary alloys for bio-medical applications. Proceeding of 8th International Conference on Magnesium Alloys and Their Applications, Wiley-VCH, DGM, Weinheim 2009, 1182–1188
17 Witte F, Fischer J, Nellesen J, *et al. In vitro* and *in vivo* corrosion measurements of magnesium alloys. Biomaterials, 2006, 27: 1013–1018
18 Witte F, Abeln I, Switzer E, *et al.* Evaluation of the skin sensitizing potential of biodegradable magnesium alloys. J Biomed Mater Res, 2008, 86A: 1041–1047
19 Witte F, Fischer J, Nellesen J, *et al. In vivo* corrosion and corrosion protection of magnesium alloy LAE442. Acta Biomater, 2010, 6: 1792–1799
20 Hort N, Huang Y, Fechner D, *et al.* Magnesium alloys as implant materials-principles of property design for Mg-RE alloys. Acta Biomater, 2010, 6: 1714–1725
21 Luo S, Zhang Q, Zhang Y, Li C, Xu X, Zhou T. *In vitro* and *in vivo* studies on a MgLi-X alloy system developed as a new kind of biological metal. Mater Sci Forum, 2013, 748, 257–263
22 Zeng RC, Qi WC, Song YW, *et al. In vitro* degradation of MAO/PLA coating on Mg-1.21Li-1.12Ca-1.0Y alloy. Front Mater Sci, 2014, 8: 343–353
23 Nene SS, Kashyap BP, Prabhu N, *et al.* Microstructure refinement and its effect on specific strength and bio-corrosion resistance in ultralight Mg-4Li-1Ca (LC41) alloy by hot rolling. J Alloys Compd, 2014, 615: 501–506
24 Zeng RC, Qi WC, Cui HZ, *et al. In vitro* corrosion of as-extruded Mg-Ca alloys-the influence of Ca concentration. Corrosion Sci, 2015, 96: 23–31
25 Li Z, Gu X, Lou S, *et al.* The development of binary Mg-Ca alloys for use as biodegradable materials within bone. Biomaterials, 2008, 29: 1329–1344
26 Liu R, Jiang K, Zhao BD, et al. *In vitro* biocompatibility and bioactivity of a new medical Mg-Li-Ca alloy. Chin J Tissue Eng Res, 2014, 52, 8409–8413
27 Zeng R, Qi W, Zhang F, *et al. In vitro* corrosion of Mg-1.21Li-1.12Ca-1Y alloy. Prog Nat Sci-Mater Int, 2014, 24: 492–499
28 Cui LY, Gao SD, Li PP, *et al.* Corrosion resistance of a self-healing micro-arc oxidation/polymethyltrimethoxysilane composite coating on magnesium alloy AZ31. Corrosion Sci, 2017, 118: 84–95
29 Cui LY, Hu Y, Zeng RC, *et al.* New insights into the effect of Tris-HCl and Tris on corrosion of magnesium alloy in presence of bicarbonate, sulfate, hydrogen phosphate and dihydrogen phosphate ions. J Mater Sci Tech, 2017
30 Haferkamp H, Niemeyer M, Boehm R, *et al.* Development, processing and applications range of magnesium lithium alloys. Mater Sci Forum, 2000, 350-351: 31–42
31 Wang J, Witte F, Xi T, *et al.* Recommendation for modifying current cytotoxicity testing standards for biodegradable magnesium-based materials. Acta Biomater, 2015, 21: 237–249
32 Bodansky M. The effect of hydrogen ion concentration on saponinhemolysis. J Biol Chem, 1929, 82: 567–577
33 Li RC. Effect of metal ions on human red blood cell membrane and its relationship with the metal ion properties. J Beijing Med Univ, 1995, 27: 239–240
34 Zeng RC, Chen J, Ke W, *et al.* pH value in simulated occluded corrosion cell for magnesium alloys. Trans Nonferrous Met Soc China, 2007, 17: s194–s197
35 Chen YL, Helm CA, Israelachvili JN. Molecular mechanisms associated with adhesion and contact angle hysteresis of monolayer surfaces. J Phys Chem, 1991, 95: 10736–10747

36 Li YC, Li MH, Hu WY, *et al.* Biodegradable Mg-Ca and Mg-Ca-Y alloys for regenerative medicine. Mater Sci Forum, 2010, 654-656: 2192–2195
37 Minárik P, Král R, Pešička J, *et al.* Evolution of mechanical properties of LAE442 magnesium alloy processed by extrusion and ECAP. J Mater Res Tech, 2015, 4: 75–78
38 Seitz JM, Collier K, Wulf E, *et al.* The effect of different sterilization methods on the mechanical strength of magnesium based implant materials. Adv Eng Mater, 2011, 13: 1146–1151
39 Yan H, Chen R, Han E. Microstructures and mechanical properties of cold rolled Mg-8Li and Mg-8Li-2Al-2RE alloys. Trans Nonferrous Met Soc China, 2010, 20: s550–s554
40 Li H, Yao G, Guo Z, *et al.* Microstructure and mechanical properties of Mg-Li alloy with Ca addition. Acta Metall Sin (Engl Lett), 2006, 19: 355–361
41 Haferkamp H, Boehm R, Holzkamp U, *et al.* Alloy development, processing and applications in magnesium lithium alloys. Mater Trans, 2001, 42: 1160–1166
42 Ward CA, Stanga RD, Zingg W, Herbert MA. Relation of proteins, platelets, and gas nuclei in adhesion to a synthetic material. Am J Physiol, 1977, 233: H100–H105
43 Oliveira R, Azeredo J, Teixeira P, Fonseca AP. The role of hydrophobicity in bacterial adhesion. Bioline, 2001, 11–22
44 Daffonchio D, Thaveesri J, Verstraete W. Contact angle measurement and cell hydrophobicity of granular sludge from up flow anaerobic sludge. Appl Environ Microbiol, 1995, 61: 3676–3680
45 Bumgardner JD, Wiser R, Elder SH, *et al.* Contact angle, protein adsorption and osteoblast precursor cell attachment to chitosan coatings bonded to titanium. J BioMater Sci Polymer Ed, 2003, 14: 1401–1409
46 Li N, Zheng Y. Novel magnesium alloys developed for biomedical application: a review. J Mater Sci Tech, 2013, 29: 489–502
47 Yin ZZ, Zeng RC, Cui LY, et al. Progress on phosphate coatings on biodegradable magnesium alloys. J Shandong Univ Sci and Technol, 2017, 36: 57–69
48 Cui LY, Zeng RC, Li SQ, *et al.* Corrosion resistance of layer-by-layer assembled polyvinylpyrrolidone/polyacrylic acid and amorphous silica films on AZ31 magnesium alloys. RSC Adv, 2016, 6: 63107–63116

Acknowledgements This work was supported by the National Natural Science Foundation of China (51571134), the Scientific Research Foundation of Shandong University of Science and Technology (SDUST) for Recruited Talents (2013RCJJ006), SDUST Research Fund (2014TDJH104), and Joint Innovative Center for Safe and Effective Mining Technology and Equipment of Coal Resources. Thanks also go to Prof. Rongshi Chen at the Institute of Metals Research, Chinese Academy of Sciences for his preparation for the alloys.

Author contributions Cui L and Sun L performed the experiments; Cui L and Sun L wrote the paper with support from Zeng R and Zheng Y. All authors contributed to the general discussion.

Conflict of interest The authors declare that they have no conflict of interest.

Lanyue Cui is currently a PhD student at the College of Materials Science and Engineering, Shandong University of Science and Technology. She was born in Zibo, Shandong province, China in 1991. She received her Bachelor's degree from Shandong University of Science and Technology in 2014. Her research interests are focused on the corrosion and protection of magnesium alloys.

Rongchang Zeng is currently a professor at the College of Materials Science and Engineering, Shandong University of Science and Technology. He received his PhD degree in materials science from the Institute of Metal Research, Chinese Academy of Sciences in 2003. From March 2006 to March 2007, he was a visiting scientist in the Institute of Materials Research of HZG (GKSS). His research focuses on the corrosion and protection of metals and degradable biomedical magnesium alloys.

Yufeng Zheng received his PhD in materials science from Harbin Institute of Technology, China in 1998. Since 2004, he has been a full professor at Peking University in Beijing, China. His research focuses on the development of various new biomedical metallic materials (biodegradable Mg, Fe and Zn based alloys, β-Ti alloys with low elastic modulus, bulk metallic glass, ultra-fine grained metallic materials, etc.).

Mg-Li-Ca合金的体外降解行为与生物相容性: 锂元素含量的影响

崔蓝月[1,2†], 孙麓[1,2†], 曾荣昌[1,2*], 郑玉峰[3*], 李硕琦[1,2]

摘要 基于良好的延展性, Mg-Li基合金作为潜在的生物材料, 引起了大家的广泛注意. 由于锂元素的存在, Mg-Li二元合金表现出较低的机械强度与人们对其生物相容性的担忧. 而在 Mg-Li 合金中添加钙元素则有利于提高其机械强度与生物相容性. 本文中, 通过光学显微镜、X射线衍射、拉力拉伸、浸泡实验以及电化学极化测试等综合评估了三种类型 (α, α+β, β) 的挤压态Mg-Li (1, 9 以及15 wt.%)-1Ca 合金的微观结构、力学性能以及腐蚀行为. 体外生物相容性通过细胞毒性、溶血以及凝血四项表征. 结果表明, Mg-1Li-1Ca 和 Mg-15Li-1Ca 合金分别由 α-Mg、β-Li 以及 Mg_2Ca 相构成; 而 Mg-9Li-1Ca 则由α-Mg、β-Li双相以及 Mg_2Ca 相构成. Mg-1Li-1Ca 合金表现出最高的最大抗拉强度和屈服强度, 但其延伸率最低, 仅为10.1±1.24%; Mg-9Li-1Ca 合金的延伸率最高, 为52.2±0.01%. 长时间浸泡实验表明, 随着锂元素含量的增加, 合金的耐蚀性逐渐降低. 毒性试验结果表明, 在10%浸提液中 Mg-Li-Ca 合金对 L-929 细胞无明显毒性反应. Mg-1Li-1Ca 表现出人体可以接受的溶血率. 凝血四项实验结果指出, 除 Mg-15Li-1Ca 外, Mg-1Li-1Ca 和 Mg-9Li-1Ca 合金无促凝性反应产生.

